Extraction of morphological quantities from a digitized medium

David A. Coker[a),b)] and Salvatore Torquato[c)]
Princeton Materials Institute and Department of Civil Engineering and Operations Research, Princeton University, Princeton, New Jersey 08544

(Received 15 August 1994; accepted for publication 5 January 1995)

We present an analysis of the effect of digitization at a moderate resolution on the determination of various morphological quantities for a model three-dimensional digitized medium. Specifically, we study systems of digitized overlapping spheres which have many of the features found in man-made and geologic materials. The goal of this paper is to demonstrate which quantities are most sensitive to the process of digitization and resolution. In addition, the question of whether three-dimensional data sets are necessary to obtain reliable results concerning material structure is answered in the affirmative. © *1995 American Institute of Physics.*

I. INTRODUCTION

A fundamental understanding of the effective transport, electromagnetic and mechanical properties of random heterogeneous materials, such as porous media and composite materials, rests on the ability to characterize quantitatively the microstructure or morphology of the media. Indeed, complete characterization of the effective properties requires knowledge of an infinite set of n-point statistical correlation functions. [1–3] In practice, only lower-order morphological information is obtainable either experimentally or theoretically. Using lower-order information, one can construct rigorous bounds on a variety of effective properties of random media.[1–12] The improved bounds can be highly predictive, but they are only useful if the necessary correlation functions are readily available. For many real materials this is indeed not the case as the underlying microstructure is only partially known *a priori*.

With recent experimental advances in fields such as scanning and transmission electron microscopy,[13] scanning tunneling electron microscopy,[14] and synchrotron based tomography,[15] it is possible to obtain high resolution two- and three-dimensional microstructural phase information of a given sample. In addition, these methods are nonintrusive leaving the sample intact and unaltered, allowing complimentary studies either by any of the above techniques or through direct experimental measurement of the same sample.

Since experimental or digitized data is of finite resolution, it is important to understand the relationship between the correlation function extracted or measured from a digitized representation and the correlation function for the actual material. To understand the effect of resolution on determining correlation functions and resulting property estimates for a digitized medium, we will study (as did Berryman[8]) digitized representations of the *continuum model of overlapping spheres* at various resolutions and volume fractions. In this isotropic model, spheres are spatially uncorrelated and thus are allowed to overlap to form clusters. We choose this model for several reasons. First, for sphere volume fractions between 0.3 and 0.97, the system is bicontinuous (i.e., both the sphere space and the space exterior to the spheres percolate)[16] and thus represents a rich topology. The formation of very large "clusters" in particle systems can have a dramatic influence on the macroscopic properties of the media. Second, in many cases, the correlation functions as well as the property estimates based on this information are known either exactly or with very high precision for this model. [17–19] Thus, overlapping spheres serve as a useful benchmark investigation. Third, lessons learned from this study can be applied to better interpret morphological information extracted from digitized images of real samples.

We shall ascertain a number of different correlation functions, some of which are experimentally obtainable from lineal, plane, and/or volume measurements. The most basic and simplest quantities are the *volume fraction of phase i*, ϕ_i, and *specific surface* (the interfacial surface area per unit volume), s. These quantities are actually one-point correlation functions. For example, in the case of a statistically homogeneous system, ϕ_i is equal to the probability of finding a point in phase i. Both ϕ_i and s can be obtained from lineal, plane or volume measurements.[20–22] For isotropic media, the *two-point probability function* $S_2(r)$ gives the probability of finding the end points of a line segment of length r in one of the phases and can be experimentally obtained from a plane measurement. More generally, the n-point function $S_n(\mathbf{x_1},\ldots,\mathbf{x_n})$ gives the probability of finding n points at positions $\mathbf{x_1},\ldots,\mathbf{x_n}$ all in one phase and is fundamental to the study of the conductivity,[1–3,6] elastic moduli,[6] trapping rate,[5,9] and fluid permeability[5,7,10] of heterogeneous media.

An interesting and useful statistical measure is what has been referred by Lu and Torquato[23,24] to as the *lineal-path function* $L(z)$. This quantity is the probability that a line segment of length z is wholly in one phase or, equivalently, the probability that a point can move along a lineal path of length z in that phase without passing through the other phase. It is clear that $L(z)$ can be extracted from a lineal measurement. For three-dimensional systems, we observe that $L(z)$ is actually also equivalent to the area fraction of phase i measured from the projected image of a three-dimensional slice of thickness z onto a plane. A quantity related to $L(z)$ is the *chord-length distribution* $p(z)$[25–27]

[a)]Electronic mail: coker@astro.sunyit.edu
[b)]Permanent address: Dept. of Math & Science, SUNY Institute of Technology, Utica, NY 13504.
[c)]Electronic address: torquato@matter.princeton.edu

which gives the distribution of chord lengths. Chords are the lengths between intersections of line with the two-phase interface. Both $L(z)$ and $p(z)$ are of importance in transport problems involving discrete free paths (e.g., Knudsen diffusion and radiative transport)[28–30] and flow in porous media.[31]

Another two-point function of basic importance for porous materials is the so-called *pore size distribution* $P(\delta)$. The quantity $P(\delta)d\delta$ gives the probability that a point in the pore phase (say phase 1) lies at a distance between δ and $\delta+d\delta$ from the nearest point on the pore-solid interface. Thus, $P(\delta)$ measures and reflects connectedness information about spherical regions of radius δ and hence is an intrinsically three-dimensional measure, i.e., it cannot be obtained from a plane measurement.[21] The pore size distribution naturally arises in diffusion and reaction in heterogeneous media[11] as well as flow in porous media.[22]

Another important measure is the so-called *coarseness* C which describes local volume fraction fluctuations in the system.[25] The coarseness gives a measure of the uniformity of coverage of the phases.

All of the aforementioned quantities will be extracted from digitized representations of overlapping spheres and compared to exact results. For the class of models consisting of any interacting system of spheres (overlapping or not), all of these statistical correlation functions are actually special cases of the general n-point distribution function H_n introduced by Torquato[12] from which one can exactly evaluate all of the aforementioned correlation functions.[19] We shall also evaluate several length scales associated with the different statistical measures.

Finally, a key geometrical parameter ζ_2 that determines rigorous bounds on the effective conductivity[1,3,6] and bulk modulus[1,6] of composites shall be directly computed. The parameter ζ_2 is a multi-dimensional integral over the three-point probability function $S_3(x,y,z)$. However, this is not accomplished by measuring $S_3(x,y,z)$ for all possible values if its arguments (which would require considerable computing time and memory) and then carrying out the integration. Instead, a new algorithm based on the work of Smith and Torquato[32] is presented that computes the appropriate integral over $S_3(x,y,z)$ directly.

It should be noted that the purpose of this project is the development of quick and efficient algorithms that can extract the desired morphological quantities to within 5%–10%, but in several cases, the algorithm presented is much more accurate. This degree of accuracy is sufficient as many of the improved bounds for bulk properties which rely on these quantities for input are not extremely sensitive to uncertainties in the morphological quantities. In addition, the algorithms presented here are all designed such that they are easily extended to run on parallel architectures. This is accomplished by working with individual slices of a digitized three-dimensional sample. As many of the quantities described in this investigation may be obtained from a single two-dimensional slice, many slices may be analyzed in parallel with the results averaged in the end. For quantities extractable only from fully digitized three-dimensional data, parallelization is also possible and has been accomplished, but not in the same direct manner. Further details regarding parallel implementations will not be given, but reserved for a future publication.

The paper is organized as follows. The relevant morphological are precisely defined and discussed in Sec. II. In Sec. III, several aspects of the digitization process are discussed, including the definition of the digitized spheres used in this study.[33] The algorithms used to compute the morphological quantities are described in detail in Sec. IV. Section V contains the simulation and theoretical results for systems of randomly overlapping spheres. A discussion of the results and their implications follows in Sec. VI.

II. DEFINITION OF IMPORTANT MORPHOLOGICAL QUANTITIES

The random medium is a domain of space $V(\omega) \in \mathscr{R}^3$ where the realization ω is taken from some probability space of volume V which is composed of two regions or phases: phase 1 region $\mathscr{V}_1$ of volume fraction ϕ_1 and phase 2 region $\mathscr{V}_2$ of volume fraction ϕ_2. Let $\partial\mathscr{V}$ denote the surface or interface between $\mathscr{V}_1$ and $\mathscr{V}_2$. For a given realization ω, the characteristic function $I(\mathbf{x})$ of phase 1 is given by

$$I(\mathbf{x})=\begin{cases}1 & \text{if } \mathbf{x}\in\mathscr{V}_1\\ 0 & \text{if } \mathbf{x}\in\mathscr{V}_2\end{cases}. \tag{2.1}$$

The characteristic function $M(\mathbf{x})$ for the interface is defined as

$$M(\mathbf{x})=|\nabla I(\mathbf{x})|. \tag{2.2}$$

A. *n*-point probability functions

The simplest morphological measures are the one-point correlation functions such as the volume fraction ϕ_i of phase i and the specific surface area s both of which are defined in terms of the appropriate characteristic functions as

$$\begin{aligned}\phi_1&=\langle I(\mathbf{x})\rangle,\\ s&=\langle M(\mathbf{x})\rangle.\end{aligned} \tag{2.3}$$

Here $\langle\rangle$ denotes ensemble averaging. Under the ergodic hypothesis, ensemble averaging can be replaced with volume averaging. The volume fraction ϕ_i has a simple probabilistic interpretation; it is the probability of finding a point in phase i.

The probability that two points separated by $\mathbf{r}$ both lie in the void phase is denoted by $S_2(\mathbf{r})$. For isotropic media, the two-point probability function depends only on the magnitude of the separation r and is given by

$$S_2(r)=\langle I(\mathbf{x}_1)I(\mathbf{x}_1+\mathbf{r})\rangle, \tag{2.4}$$

where $r=\|\mathbf{r}\|$. Some important properties of $S_2(r)$ are

$$\begin{aligned}&S_2(0)=\phi_1\\ &\lim_{r\to\infty} S_2(r)=\phi_1^2\\ &\frac{d}{dr}S_2(r)|_{r=0}=-\frac{1}{4}s.\end{aligned} \tag{2.5}$$

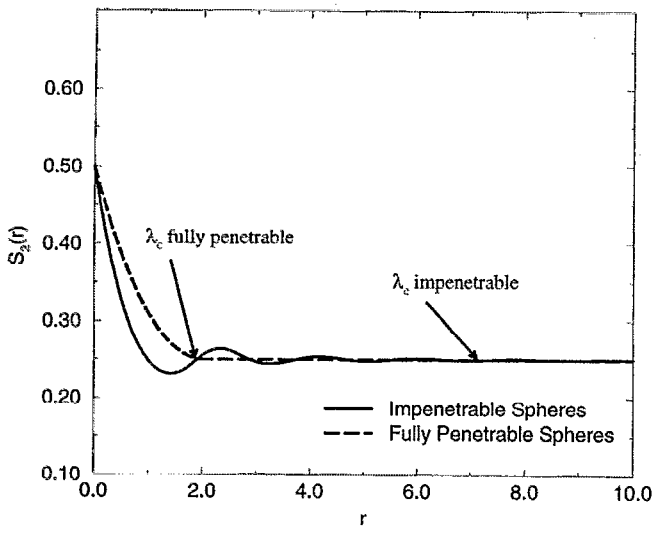

FIG. 1. Illustration of correlation length λ_C for a system of fully penetrable spheres (dashed line) using (2.9) from Ref. 17 and a system of impenetrable spheres (solid line) using data from Ref. 40.

More generally, the material's microstructure can be characterized by the n-point probability functions, S_n. $S_n(\mathbf{x}_1,\mathbf{x}_2,\ldots,\mathbf{x}_n)$ gives the probability of finding n points in the same phase at the positions, $\mathbf{x}_1,\ldots,\mathbf{x}_n$. Using the characteristic function defined above, the probability of n randomly chosen points lying in phase 1 is given by

$$S_n(\mathbf{x}_1,\mathbf{x}_2,\ldots,\mathbf{x}_n)=\langle I(\mathbf{x}_1)I(\mathbf{x}_2)\ldots I(\mathbf{x}_n)\rangle. \tag{2.6}$$

There are other n-point correlation functions and we refer readers to Ref. 3 for a thorough review.

Beran[1] mentions a characteristic length scale λ_A in terms of $S_2(r)$ as follows

$$\lambda_A=\int_0^\infty [S_2(r)-\phi_1^2]dr. \tag{2.7}$$

A quantity closely related to λ_A that appears in rigorous bounds on the fluid permeability[4] and trapping rate[9] is λ_B

$$\lambda_B=\left(\int_0^\infty [S_2(r)-\phi_1^2]r\,dr\right)^{1/2}. \tag{2.8}$$

Another length scale obtainable from the two-point function is its correlation length as defined by the distance at which the oscillations in the function $(S_2(r)-\phi_1^2)$ dwindle to zero (in practice, within 10^{-3} of zero); this scale shall be referred to as λ_C. For the case of fully penetrable spheres, λ_C is exactly equal to the sphere diameter. At the other end of the spectrum is the behavior for a system of impenetrable spheres. As seen in Fig. 1, $S_2(r)$ for impenetrable spheres oscillates appreciably about its asymptotic value of ϕ_1^2 for about 4 sphere diameters. Thus, λ_C is a length scale characterizing the short-range order due to exclusion-volume effects and is appreciably larger than a typical grain size.

As this study is concerned with the case of randomly overlapping spheres at various resolutions and volume fractions, it is appropriate to present the continuum results. In particular, overlapping spheres of radius R (taken to be phase 2) are embedded in a matrix phase (phase 1). The two-point function for the matrix phase may be written explicitly as[17]

$$S_2(r)=\begin{cases}\exp\left[-\rho\,\dfrac{4\pi}{3}\left(1+\dfrac{3r}{4R}-\dfrac{r^3}{16R^3}\right)\right] & r<2R\\ \exp\left(-\rho\,\dfrac{8\pi}{3}\right)=\phi_1^2 & r\geq 2R\end{cases} \tag{2.9}$$

where ρ is the number density (spheres per unit volume). The corresponding result for phase 2 may be written as

$$S_2^{(2)}(r)=S_2(r)+1-2\phi_1. \tag{2.10}$$

For overlapping spheres, the specific surface area is given by

$$s=\frac{3\phi_1\eta}{R} \tag{2.11}$$

where η is the reduced density,

$$\eta=\frac{4\pi}{3}\rho R^3.$$

The corresponding length scales are given explicitly by

$$\lambda_A=\int_0^{2R}\exp\left[-\rho\,\frac{4\pi}{3}\left(1+\frac{3r}{4R}-\frac{r^3}{16R^3}\right)\right]dr$$

$$\lambda_B=\left\{\int_0^{2R}\exp\left[-\rho\,\frac{4\pi}{3}\left(1+\frac{3r}{4R}-\frac{r^3}{16R^3}\right)\right]r\,dr\right\}^{1/2}$$

$$\lambda_C=2R. \tag{2.12}$$

Note that λ_C, unlike λ_A and λ_B, is independent of volume fraction in the case of overlapping spheres. This will not be true in general for arbitrary media.

B. Coarseness

An interesting quantity that has many implications in the investigation of microstructure for real materials is the *coarseness*, C, studied by Lu and Torquato.[25] This quantity provides a quantitative measure of the uniformity of the coverage of the phases. The standard deviation σ_I associated with the characteristic function I for an infinite system is a trivial constant that does not provide much useful structural information about the random medium. In particular, σ_I for fluctuations associated with the volume fraction of phase 1 is given by

$$\frac{\sigma_I}{\phi_1}=\frac{\langle I^2\rangle-\langle I\rangle^2}{\phi_1}=\frac{\phi_1-\phi_1^2}{\phi_1}. \tag{2.13}$$

In contrast, the coarseness is given in terms of the stochastic quantity $\tau(\mathbf{x})$ which is the local volume fraction of phase 1 measured in a window of finite size V_0 at $\mathbf{x}$. As to be expected $\langle\tau(\mathbf{x})\rangle=\phi_1$. Therefore, the coarseness is given by

$$C=\frac{\sigma_\tau}{\phi_1} \tag{2.14}$$

where σ_τ is the standard deviation associated with measuring τ. As a consequence of its definition, C is dependent on the volume and shape of the observation window and reduces to σ_I/ϕ_1 in the limit $V_0 \to \infty$.

In addition, Lu and Torquato[25] showed that C can be related to the two-point function described here as follows:

$$C=\frac{1}{\phi_1 V_0}\left[\int_0^\infty [S_2(r)-\phi_1^2]V_2^{int}(\mathbf{r};\sigma_0)d\mathbf{r}\right]^{1/2}. \tag{2.15}$$

Here V_0 is the volume of the observation window, $V_2^{int}(\mathbf{r};\sigma)$ is the intersection volume of two observation regions whose centroids are separated by the displacement $\mathbf{r}$, and σ_0 denotes all of the shape parameters associated with the observation region.

C. Lineal-path and chord-length distribution functions

Another important morphological descriptor is the *lineal-path function* $L(z)$[23,24] which is the probability of a finding a line segment of length z wholly in phase 1 when thrown into a sample. For a three-dimensional system, $L(z)$ is equivalent to the area fraction of phase 1 measured from the projected image of a three-dimensional slab of thickness z onto a plane. This quantity has long-standing interest in the field of stereology.

A closely related quantity is the *chord-length distribution function* $p(z)$.[26] Specifically, $p(z)dz$ is the probability of finding a chord of length between z and $z+dz$ in phase 1. Chords are distributions of lengths between intersections of lines with the two-phase interface. The first moment of $p(z)$, λ_D, mean chord length is defined as

$$\lambda_D=\int_0^\infty zp(z)dz. \tag{2.16}$$

There is a close relationship between these two quantities. Torquato and Lu[26] showed that the lineal-path function and the chord-length distribution function are related according to the expression

$$p(z)=\frac{\lambda_D}{\phi_i}\frac{d^2L(z)}{dz^2}. \tag{2.17}$$

Relation (2.11) is valid for any statistically isotropic system of arbitrary geometry.

For a system of overlapping spheres of radius R, both of these functions may be evaluated analytically [23,26] resulting in the following expressions:

$$L(z)=\phi_1^{1+(3z/4R)}$$

$$p(z)=\frac{-3}{4R}\ln(\phi_1)\phi_1^{3z/4R}. \tag{2.18}$$

Substitution of (2.18) into (2.16) leads to an expression for the mean chord length[26]

$$\lambda_D=\frac{-4R}{3\ln(\phi_1)}. \tag{2.19}$$

D. Pore-size distribution and cumulative pore-size distribution functions

The *pore-size distribution function*,[22] $P(\delta)$ is defined in such a way that $P(\delta)d\delta$ is the probability that a randomly chosen location in the pore phase (say phase 1) lies at a distance between δ and $\delta+d\delta$ of the nearest point on the pore-solid interface. Some of the interesting properties of this function are

$$\int_0^\infty P(\delta)d\delta=1 \text{ and } P(\infty)=0 \tag{2.20}$$

with

$$P(0)=\frac{s}{\phi_1}, \tag{2.21}$$

where s is the specific surface area as defined above. The moments of this function are defined in the standard way, i.e.,

$$\langle\delta^n\rangle=\int_0^\infty \delta^n P(\delta)d\delta. \tag{2.22}$$

The characteristic pore size λ_E given by the first moment

$$\lambda_E=\langle\delta\rangle=\int_0^\infty \delta P(\delta)d\delta. \tag{2.23}$$

The first moment of $P(\delta)$ provides an upper bound on the mean survival time associated with a Brownian particle diffusing through the pore phase of a system of traps.[11]

A closely related quantity is the *cumulative distribution function*, $F(\delta)$, defined as

$$F(\delta)=\int_\delta^\infty P(z)dz \tag{2.24}$$

with

$$F(0)=1 \text{ and } F(\infty)=0. \tag{2.25}$$

$F(\delta)$ is the fraction of pore space which has a pore diameter greater than δ. Consequently $1-F(\delta)$ is the fraction of pore space which excludes pores of diameter greater than δ. It should be noted that the characteristic pore-size may be defined in terms of the cumulative pore-size distribution function,

$$\lambda_E=\int_0^\infty F(\delta)d\delta. \tag{2.26}$$

The pore size distribution function for a system of overlapping spheres of radius R found by Torquato and Avellaneda[11] is given by the following equation:

$$P(\delta)=\frac{3\eta}{\phi_1 R}\left(\frac{\delta}{R}+1\right)^2\exp\left[-\eta\left(\frac{\delta}{R}+1\right)^3\right], \tag{2.27}$$

where η is the reduced density. The zero-distance limit of the pore-size distribution function for overlapping spheres is simply

$$P(0)=\frac{3\eta}{R}. \tag{2.28}$$

TABLE I. Definition of various characteristic length scales studied in this investigation.

Parameter	Definition	Equation	Description
λ_A	$\int_0^\infty [S_2(r)-\phi_1^2]dr$	(2.7)	Mean value of S_2
λ_B	$\{\int_0^\infty r[S_2(r)-\phi_1^2]dr\}^{1/2}$	(2.8)	First moment of S_2
λ_C	Range of $S_2(r)$		Correlation length
λ_D	$\int_0^\infty zp(z)dz$	(2.16)	Mean chord length
λ_E	$\int_0^\infty \delta P(\delta)d\delta$	(2.23)	Mean pore size

The cumulative distribution function for overlapping spheres is given by

$$F(\delta)=\frac{1}{\phi_1}\exp\left[-\eta\left(\frac{\delta}{R}+1\right)^3\right]. \tag{2.29}$$

Table I summarizes all of the aforementioned length scales.

E. ζ-parameter

Another geometric parameter that plays an important role in determining the bulk properties such as the effective conductivity and the bulk modulus of a random medium is ζ_2, a multi-dimensional integral over the three point probability function $S_3(y,z,\theta)$.[34] ζ_2 lies in the range [0,1] and in three dimensions is defined as follows

$$\zeta_2=1-\frac{9}{2\phi_1\phi_2}\int_0^\infty\frac{dz}{z}\int_0^\infty\frac{dy}{y}\int_{-1}^{1}d(\cos\theta)$$
$$\times P_2(\cos\theta)\left(S_3(y,z,\theta)-\frac{S_2(y)S_2(z)}{\phi_1}\right) \tag{2.30}$$

where $P_2(\cos\theta)$ is the Legendre polynomial

$$P_2(\cos\theta)=\tfrac{1}{2}(3\cos^2\theta-1). \tag{2.31}$$

The second term, $S_2(y)S_2(z)$, ensures the absolute convergence of the integral due to the singularity at the origin. This term may be omitted if a small region of size ϵ is removed in the integrals over y and z and then the limit ϵ goes to zero is taken after integrating.

Since three-point probability function $S_3(y,z,\theta)$ defines the probability of finding three points in the void phase, it may be determined from a two-dimensional image[8] rather than a full three-dimensional representation. In the introduction, it is mentioned that ζ_2 plays an important role in the construction of improved bounds for both the effective conductivity and bulk modulus; however, it should be noted that a 5% uncertainty in ζ_2 translates to only a 1% uncertainty in the predicted bounds.[8] However, this general rule is not true for either small ζ_2 or ζ_2 near its maximum value. Therefore, any algorithm returning an estimate for ζ_2 generally need only be accurate to the 10% level. This is advantageous considering the difficulty in obtaining a reliable ζ_2 or $S_3(y,z,\theta)$ from a digitized image.

III. DIGITIZED SPHERES

Since the algorithms explained in the next section are developed for the future analysis of real digitized media with a finite resolution, it is important to address the question: how does a finite resolution effect the measured correlation functions and how does this finite resolution value relate to the continuum value?

The spheres used in this study were all constructed using the following algorithm of Coker and Torquato.[33] For a single sphere centered at the origin a given voxel (cubic pixel centered at a lattice site) is either material or pore dependent on the criteria

$$x^2+y^2+z^2\leq(1+\epsilon)R^2 \tag{3.1}$$

where ϵ (a small parameter), is chosen to preserve volume. Adding this parameter to preserve volume is a very natural choice as many experimental techniques that digitize a medium rely on matching the phase volumes to other experimental measurements. In addition, previous results for typical continuum systems involving spheres are given as functions of the volume fraction or reduced density, η, which is the number of spheres per unit volume multiplied by the volume of a single trap. Therefore, by matching reduced density or volume fraction of a single sphere, our measurements closely reproduce the situation in previous studies involving continuum media. This volume preserving definition is also consistent with that used by Garboczi *et al.*[35] and Martys and Garboczi[36] in their studies of systems of nonoverlapping disks in two dimensions. It should be noted that the surface area, approximately 1.4–1.5 times greater than that of the continuum counterpart, is not affected by the value of ϵ for the diameters used in this study (greater than 10) as small adjustments in ϵ are equivalent to adding or subtracting a single cube on the surface which does not effect the surface area. Therefore, ϵ, is a convenient parameter that maintains an equivalent volume with the corresponding continuum sphere. Therefore resolution of the sphere is essentially determined by the radius, R, as the voxel size is chosen to be "1." (Increasing R corresponds to generating a more finely resolved sphere.) In Fig. 2, a sample two-dimensional projection of a typical sphere generated by the above criteria is shown.

IV. ALGORITHMS

A. Two-point probability function

The isotropic two-point probability function $S_2(r)$ is computed on a two-dimensional template such as that used in[37] and illustrated in Fig. 3 with the center of the template providing a zero-distance reference point. Even though the medium is digitized on a lattice, the center location is chosen on a continuum background. The phase of the center location is determined by choosing the phase of the nearest lattice point. This is consistent with the assumption that the material is comprised of a set of voxels (or cubes) centered at each lattice site. This is different than using a bilinear interpolation, but we believe that our method is the physically correct

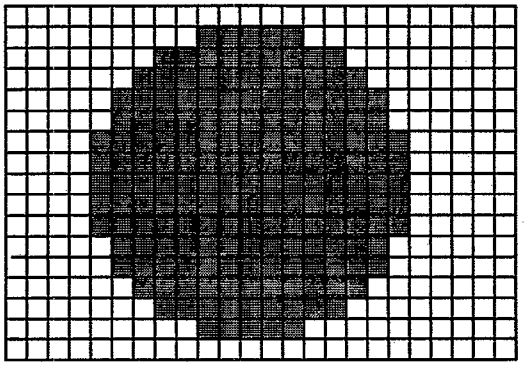

FIG. 2. Two-dimensional projection of digitized sphere with diameter = 15.

method due to the nature in which the data is digitized as discussed above. The same rule applies for determining the phase of the other template points.

The algorithm for $S_2(r)$ is constructed in two different ways. To obtain the general large scale behavior, a coarse template is used in which the distance between rings or Δr is set equal to the lattice spacing. This provides a quick algorithm that yields large scale information such as the typical grain or sphere size. For a system of overlapping spheres, $S_2(r)$ reaches its asymptotic value of ϕ_1^2 at a distance of one sphere diameter. With a more general material comprised of arbitrarily shaped phases, the distance at which the asymptotic value is obtained may be determined with this rather coarse template. In addition, the coarse template is used to obtain a fairly good estimate for the length scale λ_C. As noted above, the slope of $S_2(r)$ at the origin provides a useful measure of the specific surface area. Therefore, it is not desirable to use a coarse template as the slope at the origin will be highly sensitive to Δr. With regard to this issue, a fine-scale template is used to investigate small-scale features that provides a much more accurate measure of the specific surface area from the measure of S_2. Later the results for the specific surface area will be compared with both the continuum result and the result from an explicit measurement. The fine scale template is also used to compute both λ_A and λ_B.

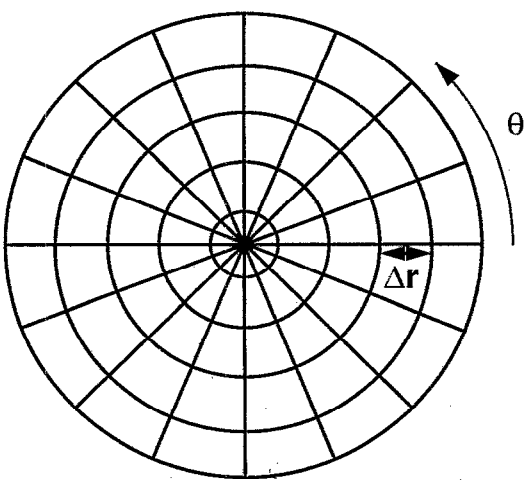

FIG. 3. Illustration of template used to compute the two point probability function $S_2(r)$.

To obtain the isotropic two-point probability function, a random location for the template center that allows for the insertion of the entire template is chosen from a flat random number generator for a given two-dimensional slice of data. $S_2(r)$ is then computed along a ray at a given angle and then averaged over all angles. This process is repeated many times for a given slice. The in-slice results are then averaged over many slices. This provides a measure of the fluctuations associated with computing $S_2(r)$ across slices while the fluctuations associated with $S_2(0)=\phi_1$ provide a direct measure of the coarseness, C. By choosing only locations that allow for the insertion of the entire template, the fluctuations of $S_2(r)$ become relatively independent of distance as each has the same number of sample points per slice.

B. Coarseness

The coarseness function is a measure of the fluctuations of the volume fraction across observation windows. Therefore, the algorithm chosen is one in which the volume fraction of the pore phase is measured for a given observation window or window(s) within a single slice and then averaged over slices. The standard deviation associated with the volume fraction measurements divided by the mean value of the volume fraction is the coarseness as discussed above. Since the coarseness has a dependence on the volume and shape of the observation window, it is important to make clear that the observation windows are rectangular slabs with thickness 1. This allows for measurement in a single slice rather than across slices. This is the typical manner in which a digitized medium is analyzed for most statistical quantities and does not impose an unwarranted bias. To the contrary, measuring C in this manner provides a direct measure of the statistics associated with either a single slice or groups of slices.

C. Lineal-path function

Computation of the lineal-path function for a digitized sample is fairly straightforward. In the approach described here, a very efficient method is used to investigate the lineal-path function that is much quicker than the more traditional direct algorithm. The algorithm described here is for the determination of the lineal-path function associated with the pore phase (phase 1). The procedure is equally applicable to other phases as well, but we shall restrict the discussion to phase 1 for clarity:

(i) Draw an oriented line through a two-dimensional slice of the sample.

(ii) Pick a random location on this line; if this point is in the void phase mark this location as point A, otherwise pick a new random location. Move along the line from point A until encountering the material phase which is labeled point B.

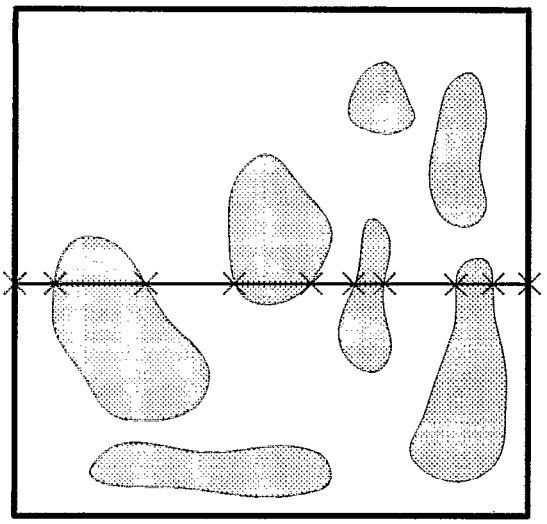

FIG. 4. Illustration of line drawn through two-dimensional slice used to compute both the lineal-path function and the chord-length distribution function.

(iii) Increment the counter associated with the distance from point A to point B and all counters associated with distances less than this length; leave counters associated with distances greater than this length unchanged.

This procedure is repeated along the initial oriented line and then repeated over many lines in an individual slice. Here the term *oriented line* means that the direction one moves from point A is always chosen to be the same direction for a given line, i.e., to the left or the right. After investigating many such lines, the counters are divided by the total number random locations chosen. This gives the probability of inserting a line segment of a specified length wholly into a single phase of the system. The result for each slice is then averaged over many slices.

A traditional algorithm would involve choosing a line segment of a given length, say l, and then trying to insert this into the system a given number of times to define the probability associated with this length. This is then repeated for each length. The *new algorithm* is much quicker since all possible lengths are probed with each measurement. This efficient approach is incorporated into many of the algorithms developed for this investigation. Due to the complex nature of a digitized medium, the actual implementation is restricted to inserting the above-mentioned lines along the horizontal, vertical, and diagonal directions only. This greatly simplifies the implementation; otherwise, it would be necessary to use methods such as those use in ray tracing to follow a line with an arbitrary orientation. This complication for arbitrary angles would exist in both the new algorithm and the more traditional method. It will be shown later that the use of only certain directions does not compromise the usefulness or accuracy of the measurements.

D. Chord-length distribution functions

The algorithm for computing the chord-length distribution function is not novel as it strictly adheres to the statistical definition given above. Again for clarity, the following algorithm refers only to an investigation of the pore phase:

(i) Draw a line through a two-dimensional slice.
(ii) Starting at the endpoint, move along the line until a pore phase voxel is found; mark this location as point A.
(iii) Beginning at point A, move along the line until encountering the material phase; mark this as point B.
(iv) The distance between point A and point B is recorded as a single chord length.
(v) Repeat the process by continuing to move along the line in the original direction starting at point B.

The process is repeated for several more lines within a slice with the list of chord-lengths recorded. The chord lengths are now binned, the bins being normalized by the total number of chords measured. As with the other algorithms this process is repeated for many slices and averaged.

In order to keep the algorithm simple and avoid the aforementioned problems associated with lines at arbitrary angles, only horizontal and vertical lines are used. This limits the minimum bin size to a single lattice spacing and precludes the investigation of chords of length less than 1 lattice spacing. Therefore, to obtain information at zero-distance, we extrapolate to the origin using a three-point Lagrange extrapolation. The accuracy and implications of this simplification are discussed later as the chord-length distribution function $p(z)$ is a probability density and is highly dependent on the resolution of the binning process.

E. Pore-size distribution function and cumulative pore-size distribution function

The pore-size distribution $P(\delta)$ function, like the chord-length distribution function, is a probability density. This function measures the probability of finding the material phase at a distance between δ and $\delta+d\delta$ from a random point chosen in the void phase. Unlike the previous quantities, the pore-size distribution function is an inherently three-dimensional quantity that cannot be obtained from a two-dimensional slice[21] since $P(\delta)$ contains some measure of connectedness. Therefore, this function is determined from a full three-dimensional digitized sample. The algorithm works in the following manner:

(i) Choose a random three-dimensional location in the pore phase.
(ii) Determine the largest sphere that just touches the material phase centered at the above location in phase 1 and record this radius.
(iii) Repeat for many locations and create a list of radii at each location.

The pore-size distribution function is then obtained by binning the sphere radii found in the second step and dividing by the total number of radii.

The cumulative pore-size distribution function measures the probability of inserting a sphere of radius r into a specified phase. This function is obtained by taking the list of radii at each location and incrementing all counters associated with radii less than or equal to a given radii. In the end, all

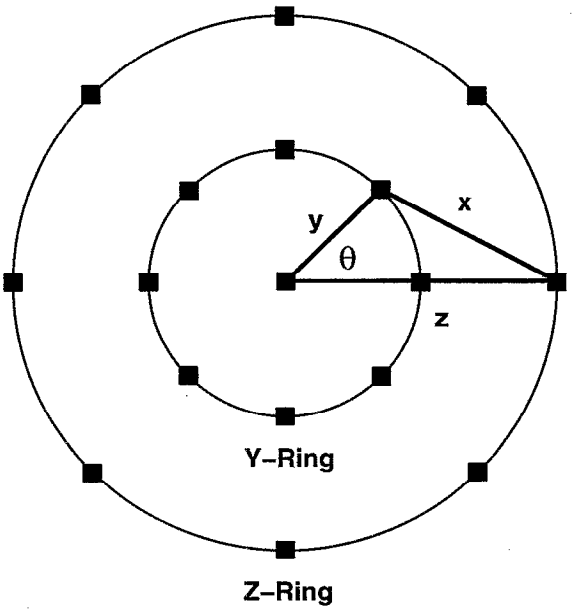

FIG. 5. Illustration of the sampling template used in measuring ζ_2 directly from the characteristic function. Note the use of concentric rings satisfying the condition $y \leq z$.

counters are divided by the total number of radii. This method of using a list of radii closely parallels the method used to determine the lineal-path function and provides a comparable speedup as the probability of inserting spheres of all possible radii is determined with each measurement.

F. ζ-parameter

Previous work[8,37] to compute ζ_2 involved two basic ideas: (1) compute $S_3(y,z,\theta)$ and then integrate to obtain ζ_2 or (2) compute ζ_2 directly without the need to obtain $S_3(y,z,\theta)$. Method (1) is the most intuitive and direct means, but obtaining $S_3(y,z,\theta)$ requires a large amount of computer memory and is computationally intensive even before performing the actual integral. The work by Greengard and Helsing[38] is a form of method (2) that relies on the use of multipole expansions. This method can be very accurate, but the sophistication of the algorithm was not appropriate for this study which is concerned with the development of simple and quick algorithms. Therefore, we choose to modify another form of method (2) developed by Smith and Torquato[32] that uses the following alternative form for ζ_2 in terms of the characteristic function $I(\mathbf{r})$

$$\zeta_2 = 1 - \frac{9}{\phi_1 \phi_2} \left\langle \int_\epsilon^\infty \frac{dz}{z} \int_\epsilon^z \frac{dy}{y} \times \int_{-1}^{1} P_2(\cos\theta) d(\cos\theta) \hat{X}_3(y,z,\theta) \right\rangle \tag{4.1}$$

where

$$\hat{X}_3(\mathbf{r}_1,\mathbf{r}_2,\mathbf{r}_3) = I(\mathbf{r}_1) I(\mathbf{r}_2) I(\mathbf{r}_3) \tag{4.2}$$

with $y = \|\mathbf{r}_2 - \mathbf{r}_1\|$, $z = \|\mathbf{r}_3 - \mathbf{r}_1\|$, and θ is the included angle between the displacements $(\mathbf{r}_2 - \mathbf{r}_1)$ and $(\mathbf{r}_3 - \mathbf{r}_1)$ as illustrated in Fig. 5. ϵ is a small nonzero parameter that regulates the divergence at the origin and it is understood that ζ_2 is obtained from the $\epsilon \to 0$ limit. An additional factor of two is obtained due to the symmetry of $\hat{X}_3(y,z,\theta) = \hat{X}_3(z,y,\theta)$ with the integral over y rewritten such that $y \leq z$. This alternative form for ζ_2 allows for a direct computation of ζ_2 without having to first compute $S_3(y,z,\theta)$. Since the integrals are given in terms of the variables y, z, and θ, the integration is performed by summing over concentric rings as shown in Fig. 5. This method has the distinct disadvantage that there are sizeable statistical fluctuations associated with each integration over the product of the three characteristic functions; therefore, the algorithm tends to exhibit rather slow convergence. However, Smith and Torquato took advantage of integrating over y and z via the method of Gaussian quadrature. This allows for the use of fewer triangles while maintaining sufficient accuracy, but the method of Gaussian quadratures relies on the implicit assumption that the underlying integrand be sufficiently smooth. Therefore, integrating over a digitized image which is non-smooth by its very nature is the reason for the slow convergence. As the purpose of the present investigation is the development of a fast efficient algorithm, this feature was deemed undesirable.

The algorithm developed for this investigation is a hybrid of these two methods. The basic pieces are listed as follows:

(i) Integrate over y, z, and θ via Gaussian quadrature methods.
(ii) Compute the product $\langle I(\mathbf{r}_1) I(\mathbf{r}_2) I(\mathbf{r}_3) \rangle$ at the points specified by the Gaussian method.
(iii) Use the known symmetries of $S_3(y,z,\theta)$ to speedup the previous step.

The new algorithm basically computes $S_3(y,z,\theta)$ only at the points specified by the Gaussian quadrature method without having to store any previous result. Thus, the integration proceeds over a function that is by its very nature implicitly smooth leading to a more quickly convergent integral. The symmetries referred to in the third step are as follows:[18]

$$\lim_{y,z \to 0} S_3(y,z,\theta) = \phi_1$$

$$\lim_{\substack{x \to 0 \\ \theta \to 0}} S_3(y,z,\theta) = S_2(y)$$

$$\lim_{\substack{x \to \infty \\ y \text{ fixed}}} S_3(y,z,\theta) = \phi_1 S_2(y)$$

$$\lim_{x,y,z \to \infty} S_3(y,z,\theta) = \phi_1^3 \tag{4.3}$$

where all possible permutations of x, y, and z are to be considered. In addition, the following two properties are used which provide a roughly 20% performance increase,

$$\int_{-1}^{1} P_2(\cos\theta) d(\cos\theta) S_2(y) = 0$$

$$\int_{-1}^{1} P_2(\cos\theta) d(\cos\theta) S_2(z) = 0. \tag{4.4}$$

The infinite-distance limits in (4.3) imply the asymptotic behavior of $S_3(y,z,\theta)$. In practice, the three-point function obtains its asymptotic value at a finite distance typically less than that of $S_2(r)$. Therefore, λ_C is a convenient length scale indicating the region of asymptotic behavior for $S_3(y,z,\theta)$. In practice, due to the use of the short-range cutoff ϵ, only the large distance asymptotic symmetries are of practical use. Since the two-point function $S_2(r)$ need only be computed once for the image, the above asymptotic properties provide a considerable speed-up. Therefore, the new algorithm presented here is both fast and reliable though technically somewhat more difficult to implement.

V. RESULTS

To confirm and test the limitations of the above algorithms for a digitized medium, realizations of overlapping digitized spheres are analyzed. Systems of overlapping spheres provide a convenient model to test the accuracy and limitations of the above algorithms, since many exact results are known for such systems. In the results that follow, a sphere with a diameter of 31 lattice units is used. It was shown by Coker and Torquato[33] that a sphere of this diameter provides a reasonably accurate representation of a sphere for the trapping problem which is much more sensitive to the resolution than the morphological quantities discussed here. In addition, this diameter allows for the analysis of digitized samples that are of significant statistical size. All of the results below are given for a system of digitized spheres in which the slices range in size from 300×300 square pixels to as much as 2000×2000 square pixels. The number of slices used for each measurement varies from 30 to 500 except where indicated otherwise. The larger slices are more useful for extracting quantities that decay over very long length scales such as the lineal-path function, chord-length distribution function and the integral for ζ_2. It is important to note that the systems investigated here are digitized lattice representations of a corresponding continuum system; therefore, the most basic length scale present is the lattice spacing which is taken to be one. This should be kept in mind when looking at dimensional quantities, such as, the specific surface area. However, when looking at digitized representations of real objects, the inherent lattice spacing is associated with some experimentally defined length scale. In synchrotron x-ray tomography this length scale is typically around 5–10 μm.

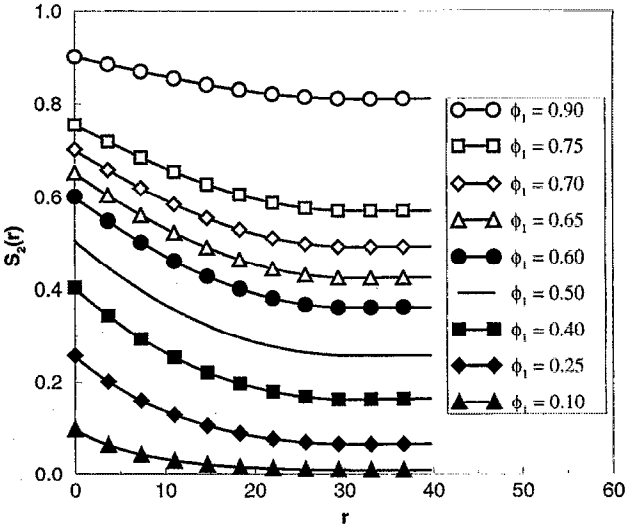

FIG. 6. Two-point probability function for a system of overlapping spheres at various void volume fractions. Every fifteenth point is marked by a symbol. On the scale of this figure, the exact theoretical results are indistinguishable from the simulation curves and therefore are not shown.

As a system of overlapping spheres exhibits various structural features at different volume fractions, a sampling of results is given for volume fractions in the range $0.10\leqslant\phi_1\leqslant0.90$. Over much of this range the system exhibits bicontinuous behavior.

A. One-point and two-point correlation functions

The two-point probability function for a system of overlapping spheres at various volume fractions is given in Fig. 6. On the scale of this figure, the results for $S_2(r)$ are indistinguishable from the exact results for the corresponding continuum system. Therefore, only $S_2(r)$ for the digitized

TABLE II. Length scales defined in Table I in units of λ_C where $\lambda_C=31$ for the systems of overlapping digitized spheres. The theoretical results correspond to systems of continuum overlapping spheres.

	λ_A		λ_B		λ_D^a		λ_E	
ϕ_1	Simulation	Exact	Simulation	Exact	Simulation	Exact	Simulation[b]	Exact
0.10	0.020±0.001	0.021	0.063±0.003	0.065	0.265	0.290	0.050	0.059
0.25	0.053±0.001	0.053	0.107±0.003	0.110	0.466	0.481	0.079	0.090
0.40	0.072±0.001	0.075	0.126±0.003	0.135	0.703	0.728	0.109	0.124
0.50	0.081±0.001	0.082	0.140±0.003	0.143	0.94	0.962	0.130	0.153
0.60	0.080±0.001	0.082	0.140±0.004	0.144	1.22	1.305	0.162	0.190
0.65	0.077±0.002	0.079	0.139±0.006	0.142	1.45	1.548	0.181	0.214
0.70	0.073±0.002	0.074	0.137±0.005	0.138	1.69	1.869	0.209	0.243
0.75	0.064±0.002	0.067	0.124±0.005	0.132	2.01	2.317	0.241	0.279
0.90	0.031±0.001	0.033	0.086±0.004	0.094	3.74	6.327	0.431	0.509

[a]The simulation values have a standard deviation of approximately 5% for the smaller volume fractions and a standard deviation of approximately 3% for the larger volume fractions.
[b]The simulation values have a standard deviation of approximately 2% due to the large volume of the digitized medium.

media are shown in Fig. 6 with an inter-ring distance $\Delta r = 1/3$ voxel. As mentioned above, the two-point probability function may be used to define the length scales, λ_A, λ_B, and λ_C. These are given in Table II. Since λ_C is the most natural length scale of the system (a sphere diameter for overlapping spheres independent of ϕ_1), all other length scales will be expressed in terms of λ_C. Even though the two-point function is visually indistinguishable from the exact continuum result, the numerical differences manifest themselves in the small discrepancies between the exact length scales and the digitized equivalents shown in Table II.

In Table III the specific surface areas for the digitized systems are given using two different methods. The digitized data consisted of 300 slices each measuring 300×300. One of the most common methods of extracting s is the use of the two-point probability function $S_2(r)$ using the third equation of (2.5). A direct measurement of the specific surface area is also possible and shown in Table III as well. The direct measurement is basically exact with a small amount of error due to finite size effects. Since the volume of the system was chosen to be sufficiently large, this error is negligible and not shown. The discrepancy between the direct measurement and the exact result is solely due to the digitized nature of the spheres. The digitized sphere (diameter 31 lattice units) used in this study has a surface area approximately 1.49 times greater than that of its continuum counterpart as discussed in Sec. III. This ratio is consistent with the data shown in Table III. The numbers shown in Table III are slightly less than expected since periodic boundary conditions are not used in the direct measurement. The specific surface area obtained from $S_2(r)$ is shown in Table III for two different resolutions. The high resolution result using $\Delta r = 0.333$ gives an s somewhere between the continuum value and the actual value. However, using a poor resolution template with $\Delta r = 1.0$ gives a result that closely approximates that of the continuum system. It should be noted however that as the resolution becomes finer and finer, the direct result will be obtained and not the continuum result. Therefore, a poor resolution template may be more desirable to extract the actual continuum s, but this also depends on the geometry of the underlying digitized medium.

TABLE III. Specific surface area s compared with the exact theoretical result (2.11). The column "Direct" refers to a voxel-by-voxel counting of surface area while the columns "$\Delta r = 1.0$" and "$\Delta r = 0.333$" refer to the use of Eq. (2.5) to obtain s from the two-point probability function, $S_2(r)$ where Δr is the distance between concentric rings for $S_2(r)$. s is given in units of inverse lattice spacing while Δr is in units of lattice spacing. The errors for the data in column 3 are all less than 2%. The errors for data in column 4 coincide with those for the data in column 5 and are therefore not given explicitly.

	s			
ϕ_1	Exact	Direct	$\Delta r = 1.0$	$\Delta r = 0.333$
0.10	0.0446	0.0625	0.0456	0.051 ± 0.001
0.25	0.0671	0.0996	0.0716	0.080 ± 0.002
0.40	0.0709	0.1038	0.0765	0.086 ± 0.002
0.50	0.0671	0.0985	0.0715	0.080 ± 0.002
0.60	0.0593	0.0869	0.0642	0.072 ± 0.002
0.65	0.0542	0.0797	0.0585	0.066 ± 0.002
0.70	0.0483	0.0709	0.0523	0.059 ± 0.002
0.75	0.0418	0.0609	0.0447	0.051 ± 0.002
0.90	0.0184	0.0276	0.0202	0.023 ± 0.001

B. Coarseness

In Fig. 7 the coarseness C is directly computed and compared to the theoretical result for 3 different volume fractions using 120 slices for each measurement. The solid line represents the exact theoretical result for continuum spheres using (2.15). The horizontal axis is the ratio of the observation window volume to the volume of a sphere with diameter λ_C. Since C is computed in a observation volume having a thickness of one slice, it provides a useful measure of the statistical fluctuations one is likely to encounter in going from slice to slice in a digitized medium. Figure 7 clearly shows that for small enough observation windows, the statistical fluctuations can be as large as 15%–20%. For very large observation windows, the dependence on the volume of the observation window is small, but nonvanishing nonetheless. As a specific example, due to the nature in which $S_2(r)$ is measured, C gives a direct measure of the statistical fluctuations associated with measuring $S_2(r)$ across multiple slices. It should be emphasized, that the data in Fig. 7 demonstrate a strong dependence on volume fraction. The results for C clearly indicate that to extract a statistically reliable result from a digitized sample, it is insufficient to examine only a single slice, even when the slice is of considerable size when compared to λ_C. Therefore, if one is examining relatively few slices, it is difficult to obtain a reliable estimate for the actual magnitude of the statistical fluctuations across slices.

C. Lineal-path and chord-length distribution functions

The lineal-path function has been computed for the material and void phases. For each volume fraction, there were

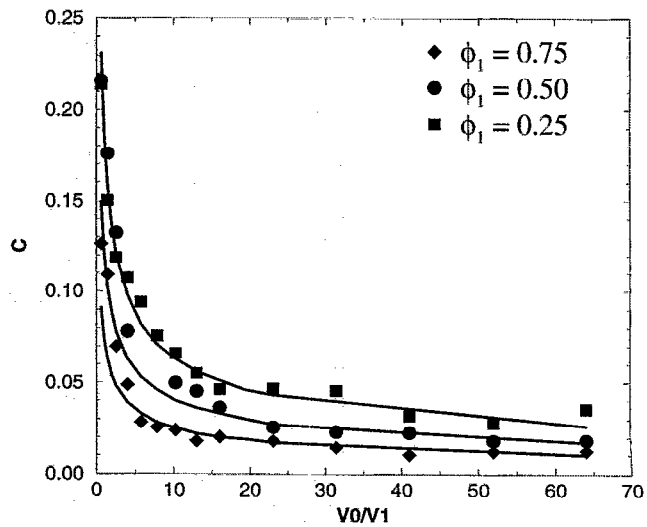

FIG. 7. C vs scaled observation window for $\phi_1 = 0.25$, 0.50, and 0.75. The solid line represents the exact theoretical result using (2.15). Here V_1 represents the volume of a sphere with diameter λ_C and V_0 represents the volume of the observation window.

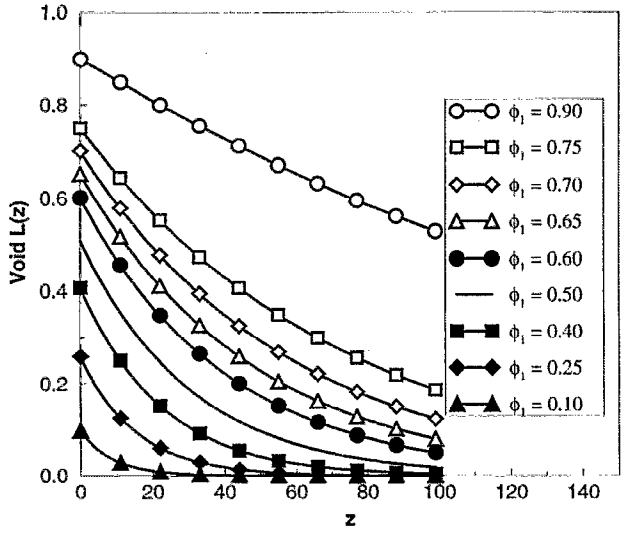

FIG. 8. Void lineal-path function for digitized spheres. Every tenth point is marked by a symbol. The horizontal axis is given in units of the lattice spacing. On the scale of this figure, the exact theoretical results are indistinguishable from the simulation curves and are therefore not shown.

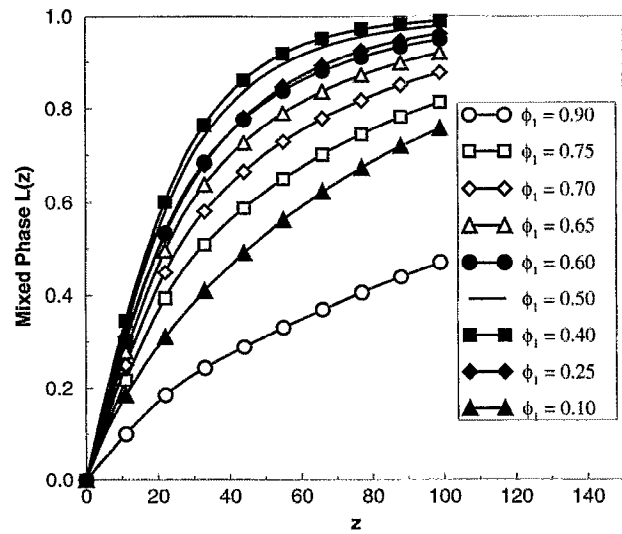

FIG. 10. Mixed-phase lineal-path function for digitized spheres. Every tenth point is marked by a symbol. The horizontal axis is given in units of the lattice spacing.

120 slices each 1000×1000. Previous exact continuum theoretical results for the void phase in a system of overlapping spheres are known; however, exact theoretical results for the material phase are not available. Due to the remarkable agreement between the exact continuum theory (not shown) and the digitized simulation for the void lineal path function (see Fig. 8), the material lineal path function (see Fig. 9) should be a relatively good approximation to the exact continuum result. This agreement between the exact theoretical result and the simulation should be considered in the same manner as that for the two-point probability function. The results show, that for high void volume fractions, the void lineal-path function is rather long-ranged demonstrating that the void phase exhibits a high degree of connectivity. In fact, the lineal-path function can be considered a crude measure of the connectivity of the sample along a lineal path. However, it should be noted that the material lineal-void function at a given packing fraction decays much quicker than the corresponding void lineal-path function at an equivalent void fraction. The mixed-phase lineal-path function gives the probability of a randomly cast line segment landing in more than one phase. As expected this function is zero at zero distance and monotonically increases to unity at large distances (see Fig. 10). Again, there are no exact theoretical results for the mixed-phase lineal-path function.

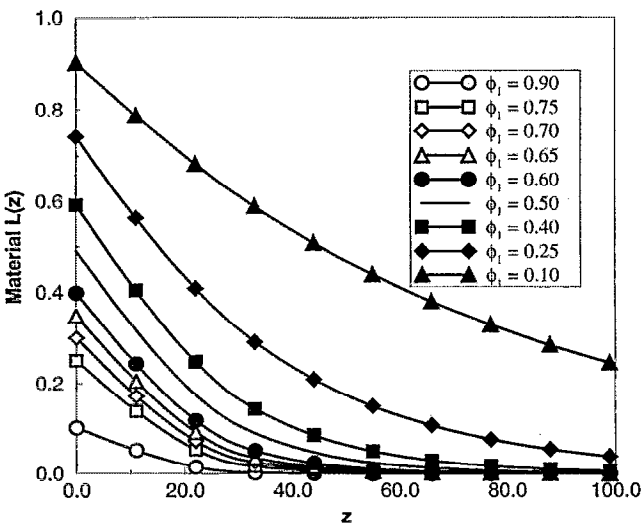

FIG. 9. Material lineal-path function for digitized spheres. Every tenth point is marked by a symbol. The horizontal axis is given in units of the lattice spacing.

The chord-length distribution function $p(z)$ for the void phase is also computed for the same slices as for the lineal-path function. The mean chord length λ_D, in units of the correlation length, is shown in Table II. Approximate errors are not given for λ_D in Table II due to the fact that this function is relatively noisy and a reliable estimate of the first moment may only be obtained after the function is averaged over many slices. However, computing λ_D for a variety of configurations shows the standard deviation to be less than 5%. As seen in Table II, the mean chord-length is always less than the continuum value. This is due to the digitized nature of the spheres which causes a relative decrease in the length of a given chord due to the non-smooth nature of the spheres as shown in Fig. 2. This is clearly illustrated in Fig. 11 where the chord-length distribution function for a digitized system with $\phi_1 = 0.25$ is compared with the exact continuum result. The digitized system exhibits a slightly larger number of short chords than the continuum system while exhibiting a slightly smaller number of longer chords than the continuum system. This difference in behavior is directly related to both the digitized nature of the medium and the use of hard boundaries, both of which increase the number of short chords. However, the major influence on the short-range behavior is the digitized nature of the spheres since the slices

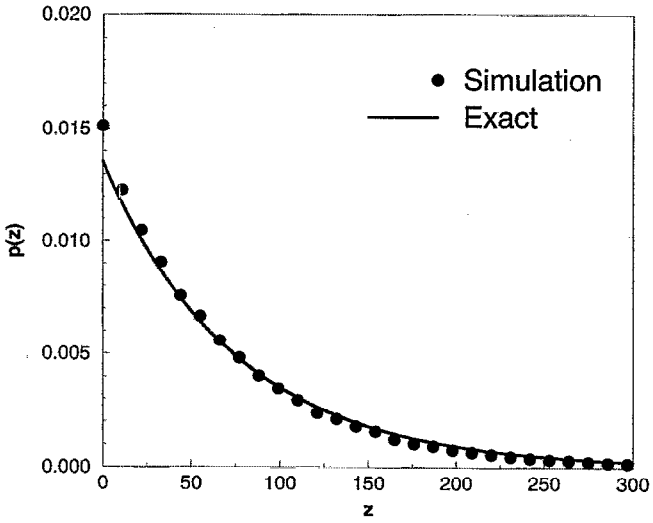

FIG. 11. Void chord-length distribution function for a system of digitized spheres with $\phi_1 = 0.25$ (filled circles) compared with the exact continuum result (solid line) from (2.18) for the same volume fraction. The horizontal axis is given in units of the lattice spacing.

are relatively large, indicating that only a small fraction of the chords in the distribution actually come from the boundary region. The general behavior illustrated in Fig. 11 is seen for all volume fractions and leads to a mean value less than that of the continuum system.

D. Pore-size distribution function and cumulative pore-size distribution function

The pore-size distribution and cumulative pore-size distribution for a volume fraction of $\phi_1 = 0.5$ are shown in Figs. 12 and 13, respectively. These figures serve to illustrate the qualitative behavior observed at the various volume fractions

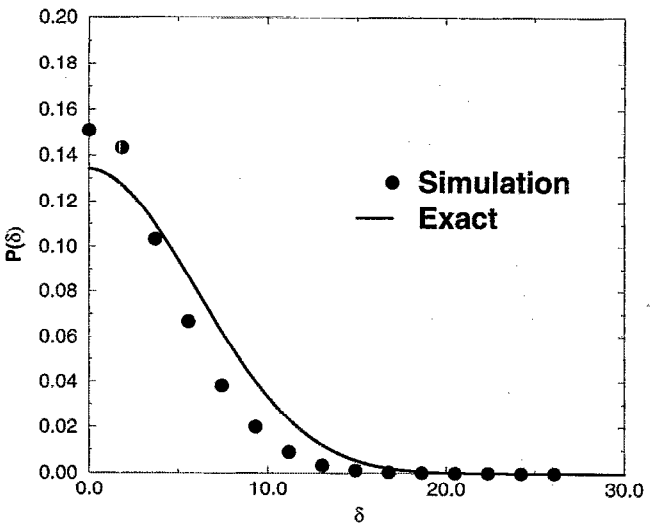

FIG. 12. Pore-size distribution function for $\phi_1 = 0.50$. The solid line is the exact theoretical expression (2.27) while the circles denote simulation data. The horizontal axis is in units of the lattice spacing.

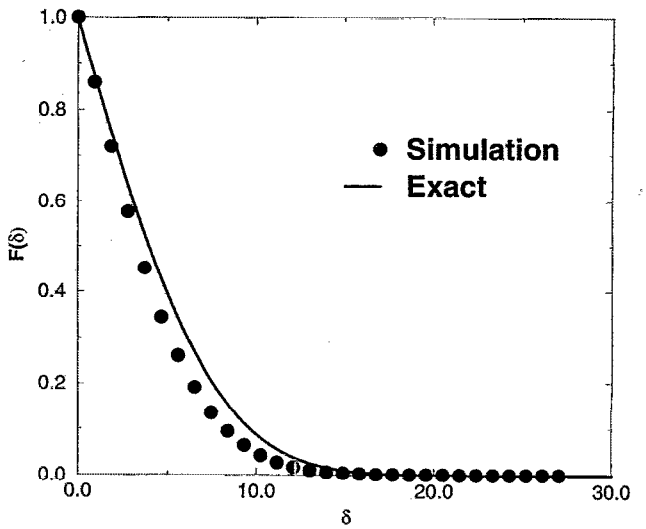

FIG. 13. Cumulative pore-size distribution function for $\phi_1 = 0.50$. The solid line is the exact theoretical expression (2.29) while the circles denote simulation data. The horizontal axis is in units of the lattice spacing.

given in Table II. The data sets were comprised of 300 slices each 300×300. For a given configuration or data set, 10^7 random points were chosen in the void phase to determine $P(\delta)$ and the first moment λ_E to provide a result with approximately 1% statistical uncertainty. In addition, λ_E was measured across different configurations with the same volume fraction which added another 1% uncertainty. Therefore, the simulation results in Figs. 12 and 13 and Table II are accurate to within 2%. Figs. 12 and 13 illustrate the difference between the exact theoretical and simulation results for λ_E in units of λ_C are shown in Table II. The fact that the simulation value for λ_E is smaller than the theoretical value is due to the different behavior at short and long distances as seen in Fig. 12. This difference in behavior is solely due to the digitized nature of the medium and not statistical uncertainty which we estimate to be approximately 2%. It should also be noted that the pore-size distribution is obtained using periodic boundary conditions in contrast to all the other quantities where hard boundary conditions were used. Therefore, hard boundary conditions (that must necessarily be used when studying real digitized material data) will increase the probability of small pores as discussed above for the chord-length distribution function.

E. ζ-parameter

The ζ-parameter for the digitized systems is compared with the exact theoretical result in Table IV. For this study, digitized slices of dimension 2000×2000 are used which provide both good statistical accuracy (as defined by the coarseness) and a reasonable maximum cut-off for both the y and z integrations. In this case a cutoff distance of 600 is seen to be sufficient for convergence. It should be noted however that this convergence is very slow. The simulation results in Table IV show good agreement with the exact theoretical results. The simulation values in Table IV have an uncertainty of approximately 5% due to a combination of fluctuations across slices and the statistical noise introduced

TABLE IV. ζ-parameter for the material phase of digitized spheres compared with the exact theoretical result[3] for various void volume fractions.

ϕ_1	Exact	ζ_2	Simulation
0.10	0.558		0.560
0.30	0.415		0.411
0.40	0.351		0.354
0.50	0.290		0.293
0.60	0.230		0.241
0.70	0.171		0.194
0.90	0.056		0.105

[a]See Reference 3.

by sampling only a finite number of triangles for a given y, z, and θ. The uncertainty due to fluctuations across slices increases somewhat for larger ϕ_1 explaining the larger discrepancies seen in Table IV for $\phi_1=0.70,0.90$. The agreement with the exact theoretical continuum result is not surprising as $S_3(x,y,z)$ is relatively insensitive to digitization in the same manner as $S_2(r)$.

VI. DISCUSSION

Here we have seen that the morphological quantities vary in their sensitivity to the digitization of the spheres. Both the two-point probability function $S_2(r)$ (along with the associated λ_A and λ_B) and the lineal-path function $L(z)$ for the digitized system differ little from their continuum results. However, the chord-length distribution function $p(z)$ and pore-size distribution function $P(\delta)$ are both sensitive to the digitization. λ_D and λ_E for the digitized system are about 10% and 15%, respectively, below their continuum values. The difference is due to the fact that $p(z)$ and $P(\delta)$ measure quantities associated with the sphere-void interface. The interface is the only quantity affected when going from a continuum to a digitized representation at a given resolution. Therefore, these quantities converge to their continuum counterparts as the resolution becomes finer and finer.

Another important point worth mentioning is the fact that the above results for $P(\delta)$ reflect the use of periodic boundary conditions. In a digitized representation of a real medium, this is no longer possible for obvious reasons. Therefore the short-range behavior seen in Fig. 12 will be enhanced for a real medium resulting in an even smaller value for λ_E.

One point often overlooked in the analysis of digitized samples is the statistical uncertainty associated with examining only one sample or slice. The results for the coarseness C clearly demonstrate that fluctuations from slice to slice may be as much as 10%–25%. This effect is non-negligible and should not be ignored. Therefore, sufficiently large volumes are required to obtain reliable results.

ACKNOWLEDGMENTS

The authors gratefully acknowledge the support of the Office of Basic Energy Science, U.S. Department of Energy under Grant No. DE-FG02-92ER14275 and the Petroleum Research Fund under Grant No. PRF-26348-AC9. They also gratefully acknowledge the support of the San Diego Supercomputer Center for the use of the Intel Paragon for the development of parallel implementations of the algorithms.

[1] M. J. Beran, *Statistical Continuum Theories* (Wiley, New York, 1968).
[2] G. W. Milton, Commun. Math. Phys. **111**, 281 (1987); **111**, 329 (1987).
[3] S. Torquato, Appl. Mech. Rev. **44**, 37 (1991).
[4] S. Prager, Phys. Fluids **4**, 1477 (1961); J. Chem. Phys. **50**, 4305 (1969).
[5] M. Doi, J. Phys. Soc. Jpn. **40**, 567 (1976).
[6] G.W. Milton, Phys. Rev. Lett. **46**, 542 (1981).
[7] J. G. Berryman and G. W. Milton, J. Chem. Phys. **83**, 754 (1985).
[8] J. G. Berryman J. Appl. Phys. **57**, 2374 (1985); J. G. Berryman and S. C. Blair, J. Appl. Phys. **60**, 1930 (1986).
[9] J. Rubinstein and S. Torquato, J. Chem. Phys. **88**, 6372 (1988).
[10] J. Rubinstein and S. Torquato, J. Fluid Mech. **206**, 25 (1989).
[11] S. Torquato and M. Avellaneda, J. Chem. Phys. **95**, 6477 (1991).
[12] S. Torquato, J. Stat. Phys. **45**, 843 (1986).
[13] S.L. Flegler, *Scanning and Transmission Electron Microscopy: An Introduction* (W.H. Freeman, New York, 1993).
[14] *Scanning Tunneling Microscopy*, edited by J. A. Stroscio (Academic, Boston, 1992).
[15] J.H. Kinney and M.C. Nichols, Ann. Rev. Mater. Sci. **22**, 121 (1992).
[16] In Ref. 12, Torquato derived exact series representations of H_n in terms of the n-particle probability density ρ_n. For overlapping spheres, ρ_n is a constant independent of sphere position, allowing an exact evaluation of H_n and hence all of the different correlation functions.
[17] H. L. Weissberg, J. Appl. Phys. **34**, 2679 (1963).
[18] S. Torquato and G. Stell, J. Chem. Phys. **79**, 1505 (1983).
[19] See Ref. 3 and references therein.
[20] E. E. Underwood, *Quantitative Stereology* (Addison-Wesley, Reading, MA, 1970).
[21] S. Torquato, Physica A **207**, 79 (1994).
[22] A. E. Scheidegger, *The Physics of Flow Through Porous Media* (University of Toronto Press, Toronto, 1974).
[23] B. Lu and S. Torquato, Phys. Rev. A **45**, 922 (1992).
[24] B. Lu and S. Torquato, Phys. Rev. A **45**, 7292 (1992).
[25] B. Lu and S. Torquato, J. Chem. Phys. **93**, 3452 (1990).
[26] S. Torquato and B. Lu, Phys. Rev. E **47**, 2950 (1993).
[27] B. Lu and S. Torquato, J. Chem. Phys. **98**, 6472 (1993).
[28] W. Strieder and S. Prager, Phys. Fluids **11**, 2544 (1968); F. G. Ho and W. Strieder, J. Chem. Phys. **70**, 5635 (1979).
[29] M. Tassopoulos and D. E. Rosner, Chem. Eng. Sci. **47**, 421 (1992).
[30] T. K. Tokunaga, J. Chem. Phys. **82**, 5298 (1985).
[31] C. E. Krohn and A. H. Thompson, Phys. Rev. B **33**, 6366 (1986).
[32] P. A. Smith and S. Torquato, J. Appl. Phys. **65** , 893 (1989).
[33] D. A. Coker and S. Torquato, J. Appl. Phys. **7**, 955 (1995).
[34] G. W. Milton, J. Mech. Phys. Solids **30**, 3790 (1982); S. Torquato, Ph. D. thesis, SUNY Stony Brook, Stony Brook, 1980.
[35] E. J. Garboczi, M. F. Thorpe, M. DeVries, and A. R. Day, Phys. Rev. A **43**, 6473 (1991).
[36] N. Martys and E. J. Garboczi, Phys. Rev. B **46**, 6080 (1992).
[37] P. A. Smith and S. Torquato, J. Comput. Phys. **76**, 176 (1988).
[38] L. Greengard and J. Helsing, J. Appl. Phys. **77**, 2015 (1995).